

# A renewable low-frequency acoustic energy harvesting noise barrier for high-speed railways using a Helmholtz resonator and a PVDF film

Yuan Wang, Xin Zhu, Tingsheng Zhang, Shehar Bano, Hongye Pan, Lingfei Qi, Zutao Zhang\*, Yanping Yuan

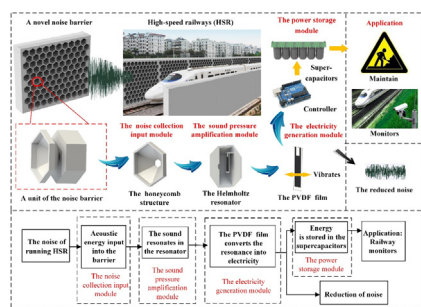
School of Mechanical Engineering, Southwest Jiaotong University, Chengdu 610031, PR China



## HIGHLIGHTS

- A novel noise barrier with a honeycomb structure was designed to harvest acoustic energy.
- The sound pressure was amplified in a Helmholtz resonator at a resonance frequency.
- A PVDF film was used to convert the energy of the sound resonance into electricity.
- The energy from the noise conversion was stored in supercapacitors to power small electronic devices.
- The tested properties are advisable for replacing a conventional noise barrier in high-speed rails.

## GRAPHICAL ABSTRACT



## ARTICLE INFO

**Keywords:**  
Acoustic energy  
Noise barrier  
Supercapacitors  
Helmholtz resonator  
PVDF  
High-speed rail

## ABSTRACT

High-speed railways have received much attention globally in recent years. While high-speed railways bring convenience to people, the environmental costs, such as noise pollution, are assignable, especially in residential areas near the railway. Notably, noise is a regenerative energy resource that can be harvested to generate electricity. Therefore, using noise barriers to simultaneously reduce noise and generate electricity is a meaningful research topic. In this paper, we present a novel renewable acoustic energy harvesting noise barrier using a Helmholtz resonator and a Polyvinylidene Fluoride (PVDF) film to convert the acoustic energy of low-frequency noise from high-speed railways into electricity. The renewable acoustic energy harvesting system scheme mainly consists of four components: a noise collection input module, a sound pressure amplification module, an electricity generator module and a power storage module. The sound pressure is amplified in a Helmholtz resonator, and a PVDF film in the electricity generator module can convert acoustic energy into electric energy. The power storage module stores the electric energy in supercapacitors that power small electronic devices, such as the monitors along the railway. Based on the experiments, one unit of the system can produce an instantaneous maximum output voltage of 74.6 mV at 110 dB (SPL), verifying the efficiency and practicability of the proposed acoustic energy harvesting noise barrier system being applied for renewable energy in high-speed railways.

\* Corresponding author.

E-mail address: [zzt@swjtu.edu.cn](mailto:zzt@swjtu.edu.cn) (Z. Zhang).

## 1. Introduction

High-speed railways (HSR) are currently considered as one of the most significant transportation modes due to their large passenger volume and high efficiency [1]. Countries all over the world are developing high-speed railway transportation, which is an essential mode of transportation in modern society [2]. Railway networks have covered large areas [3]. However, the environmental costs cannot be ignored, especially the noise pollution, such as aerodynamic noise and rolling noise generated from high-speed trains, which has become a prominent environmental issue [4]. With energy harvesting becoming increasingly promising [5], a method to use noise energy to achieve noise reduction and power generation is an interesting topic in this research field. Presently, researches on reducing noise and harvesting acoustic energy mainly focus on three existing aspects.

First, noise barriers have become a widely used technical measure for noise reduction from road and railway transportation to mitigate potentially significant noise impacts. The sound absorption, insulation and reflection performances of a noise barrier were a studies concern. Reiter et al. determined the reflection characteristics of a noise barrier, and they analysed, compared and evaluated several methods to find a model for predicting the sound reflection index (RI) of a noise barrier [6]. With the environmental assessment process, Arenas et al. described the potential problems and effects of existing environmental noise barriers [7].

Second, with increasing global energy demand, a substantial change in energy systems is necessary [8]. Researchers have been studying on alternative energy resources over the past years, and studies on the conversion of sunlight, such as photovoltaics (PV), were rapidly developed over the past few years [9]. PV power systems are presently an indispensable technology [10], and noise barriers combined with PVs have been studied for many years. Recently, deep investigations and research been performed on PV module technology due to its many advantages like energy potential, and great research progress has been made on the construction of photovoltaic noise barriers (PVNBs) [11]. Many fundamental studies have verified the implementability of PVNBs. EllenDe Schepper investigated the feasibility of a PVNB, and the Monte Carlo method was used to analyse its cost benefit. Additionally, the results showed that PVNBs are a profitable project [12]. Faturrochman et al. built a prototype of a bifacial photovoltaic noise barrier and demonstrated, through experiments, that the measured power output results agree well with the simulated power output data [13]. Gu et al. proposed and installed a complete noise barrier with a 360 m PV array along a Chinese metro railway line. The proposed PVNB can achieve a power generation of approximately 5000 kWh annually, which will avoid the emission of some harmful gases to a certain extent [14].

Third, renewable, sustainable and non-pollution sources of energy have attracted much attention, and harvesting abundant environmental energy, such as sunlight, wind, water and sound have become an extremely important part of energy utilization and recovery. Many research efforts have been devoted to technologies focusing on alternative energy harvesting or energy conversion. Zhang et al. designed a kinetic energy harvesting system to harvest power wasted by vehicles passing through a road tunnel [15]. For use in extended range electric vehicles, Zhang et al. presented a novel shock absorber to collect the wasted suspension energy from the moving vehicles [16]. Technologies of energy harvesting will be a desirable solution to energy shortages [17]. Orrego et al. developed a novel wind energy harvester by self-sustained oscillations of a flexible piezoelectric membrane fixed in an inverted orientation [18]. Helios Vocca discussed a vibration harvesting method with bi-stable oscillators to model nonlinear piezoelectric harvesters, investigating the potential of the noise driven dynamics [19]. Zhang et al. developed a portable electro-magnetic energy harvesting design that converts vibrations of railroads into electricity through mechanical transmission, and the proposed energy harvester proved through tests

to be effective with an efficiency of 55.5% [20]. The applications of piezoelectric designs are fully developed to convert vibrations to electrical energy and have captured much attention in recent years due to the superiorities of a high transduction efficiency, easy establishment and so on. An innovative energy harvesting pavement system is fully designed in [21] by Guo et al., in which the asphalt layers composed of piezoelectric materials become conductive to harvest the kinetic energy of vehicles. The maximum electric output can reach 300 mW. Roshani et al. verified the feasibility of harvesting mechanical energy of the strain and stress generated by the vehicles through the roadways. They conducted experiments to consider the potential of harvesting energy from asphalt pavements using piezoelectric materials [22]. Guan et al. proposed a piezoelectric system to harvest energy from rotational movement, such as generators integrated onto the inner surface of vehicle tires. During the rotation of the energy harvester, the repeated deformation of piezoelectric elements will be transferred to electricity, and an output energy of 83.5–825 µW is gained at rotating frequencies of 7–13.5 Hz [23]. Abdelmoula et al. evaluated low-frequency Zigzag energy harvester with torsion-bending properties, and the proposed torsion-dominant mode proved to provide a higher harvested power level, decreasing the operating frequency by 50% [24].

Although various energy resource harvesting technologies have been extensively investigated, there are neglected and wasted energies all around us. For instance, acoustic energy is a significant energy resources that is generated constantly but remains unused [25]. Sound waves are pressure vibrations that propagate in elastic media. Acoustic energy can be acquired in an environment. With autonomous micro-electromechanical systems (MEMS) rapidly, globally developing, acoustic energy harvesting (AEH) that converts environmental acoustic waves into electricity using a resonator or a transducer has become viable [26]. Zhou et al. presented an acoustic energy harvester in a bi-stable state with a flat plate that is excited to oscillate, and for a certain sound pressure level (SPL), a high voltage output was generated when reaching a coherence resonance [27]. Generally, an acoustic resonator is not only used to absorb an unexpected frequency component of a sound system but also to amplify the sound pressure in an acoustic field at a specific frequency band [26]. As an efficient device for noise control, Helmholtz resonators (HRs) are one of the most universally used acoustic resonators [28]. Liu et al. studied the progress of an acoustic energy harvesting device using an electro-mechanical Helmholtz resonator (EMHR), which mainly consists of a cavity, an orifice, and a diaphragm of piezoelectric materials. For an incident SPL of approximately 160 dB, the output power can be up to approximately 30 mW which is adequate to power many low power electronic devices [29]. Yuan et al. suggested a focus on increasing the output power of acoustic energy gathering due to the low sound intensity and proposed a special design for harvesting acoustic energy. The proposed high-performance system is mainly composed of a HR with an unfixed bottom, which is appropriate for low-frequency sound waves [30]. Kim et al. developed an acoustic energy scavenger to use large amplitude acoustic waves, which was developed in response to the air that flows across the opening of a HR [31]. Noh et al. proposed a piezoelectric cantilever integrated within a HR. To maximize the efficiency of energy harvesting, the mechanical resonance of the piezoelectric cantilever was in accordance with acoustic resonance of the HR [32].

Despite the existing approaches having partly covered the problems of noise pollution and noise energy waste, certain aspects of HSR noise have not been addressed yet. Two main facts about the technology still challenge researchers: (1) Noise insulation and absorption have been emphasized but harvesting noise energy to power small electronic equipment is neglected in HSR. (2) The popularity of HSR requires better performances of noise barriers on noise reduction, especially for low-frequency noise that mostly escape the existing noise barriers along HSR. To follow up and address the aforementioned problems we proposed, in this paper, a novel noise barrier that harvests alternative acoustic energy using a HR and a Polyvinylidene Fluoride (PVDF) film

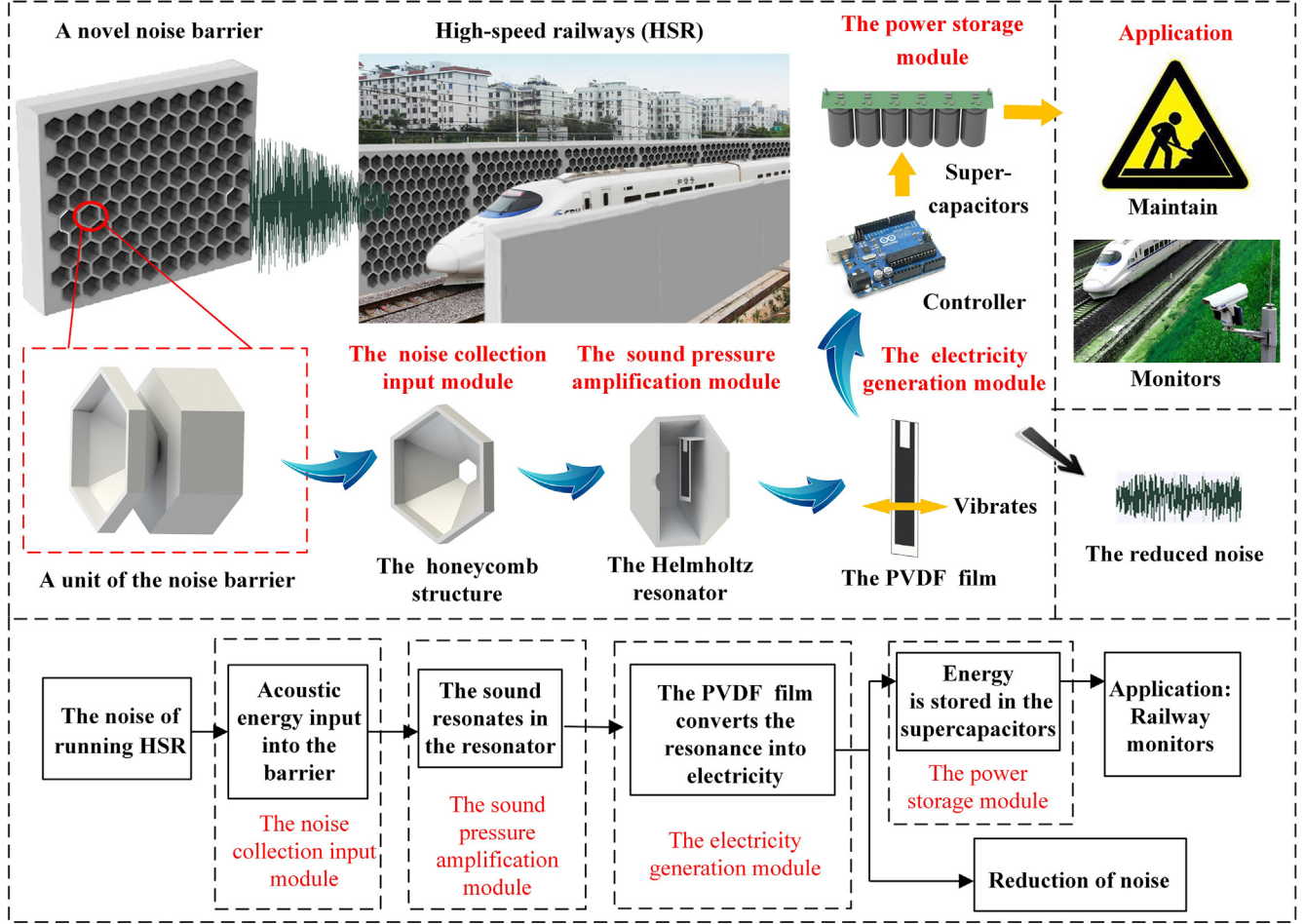


Fig. 1. Architecture of the acoustic energy harvesting noise barrier.

for HSR transportation to both achieve noise reduction and electricity generation. Supercapacitors are used in the system for energy storage to power some small electronic devices and serve as standby power supplies along the HSR, such as railway monitors and maintenance.

The rest of this paper is generally structured as follows. In Section 2, the design of the noise barrier system is described, including the noise collection input module, the resonant pressure amplification module, the electricity generator module and the energy storage module. A description of the modelling and analysis of the system is presented in Section 3. Then, the experimental details are described in Section 4. In Section 5, results and discussion are presented to verify the feasibility of the system, and further applications are described. Finally, the conclusion is given in Section 6.

## 2. System design

The general architecture of the proposed novel acoustic energy harvesting noise barrier (AEHNB), as shown in Fig. 1, consists of four parts: the noise collection input module, the sound pressure amplification module, the electricity generation module and the power storage module. The noise along the HSR is collected through the honeycomb structure and is input into the noise barrier. This is called the noise collection module. Then, the noise enters the HR, which is called the sound pressure amplification module, resonating at a certain frequency. Meanwhile, the PVDF film converts the resonance into electricity, which is called the electricity generation module. The energy is stored in supercapacitors, which are called the power storage module. Therefore, the system can simultaneously achieve the effects of both noise reduction and power generation.

The proposed renewable acoustic energy harvesting noise barrier is formed by an array of acoustic energy harvesting units (AEHUs). In this paper, one unit was selected as the research object to describe the performance of the proposed system. The prototype of the AEHU is shown from different views in Fig. 2.

### 2.1. Resonant pressure amplification module

The resonant pressure amplification module is the core part of the AEHU, and the HR is used for sound resonance and sound pressure amplification. The highest sound pressure is generated from the sound resonance. When the incident sound frequency is the same as the basic resonance frequency, which is a function of the HR's cavity volume and the neck dimensions [33]. In this paper, a hexagonal prism cavity is designed as the HR to match the advantages of the honeycomb structure. The exit of the honeycomb-like structure is connected to the neck part of the HR. When the noise reaches to the HR through the honeycomb-like structure and the neck, the sound near the basic resonance frequency will amplify the sound pressure. Fig. 3 shows the theoretical model and the prototype structure of the HR. Liu et al. investigated the acoustic properties of porous polycarbonate material (PPM), and better sound absorption effect was achieved in the low frequencies compared to conventional materials [34]. Therefore, the polycarbonate material is used to form the system cavity due to its effective sound absorption.

### 2.2. Electricity generator module

The acoustic energy conversion mechanism is the sound vibrations acting on the piezoelectric material. PVDF is the preferred piezoelectric

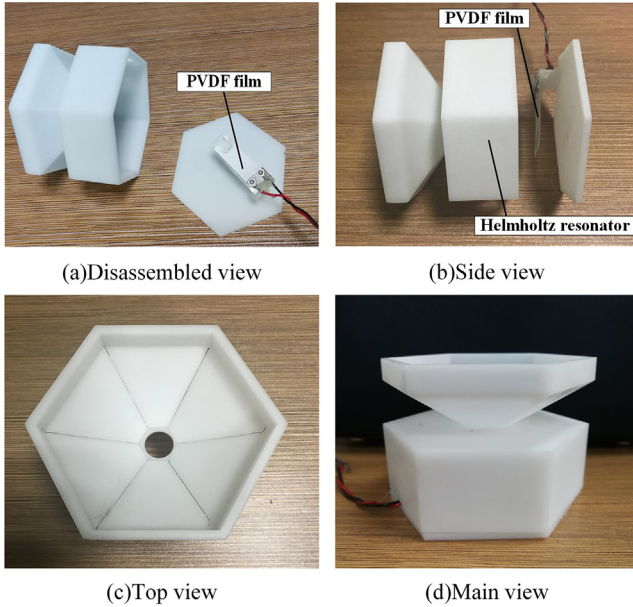


Fig. 2. Prototype of the AEHU.

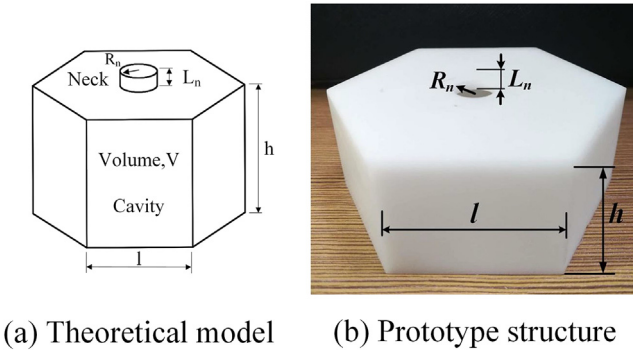


Fig. 3. Model of the Helmholtz resonator.

**Table 1**  
Properties of PVDF film (LDT-028 k/L by Measurement).

Parameter	Value
Height $h$	4.1 cm
Width $w$	1.6 cm
Thickness $t$	0.2 mm
Piezo strain constant $d_{31}$	23 pC/N
Young's Modulus $Y$	2–4 GPa
Capacitance $C_p$	380 pF/cm <sup>2</sup>
Relative permittivity $\epsilon/\epsilon_0$	12–13
Coupling factor $k$	0.14
Damping ratio $\zeta$	0.05

material due to its flexibility, low density, low impedance and high voltage electrical constant. The representative piezoelectric and physical characteristic parameters of the PVDF film considered in this paper are listed in Table 1, including the height  $h$ , width  $w$ , thickness  $t$ , piezo strain constant  $d_{31}$ , relative permittivity  $\epsilon/\epsilon_0$ , dielectric constant  $E$  and Young's modulus  $Y$  [35].

In the electricity generator module, the PVDF film is mounted at the bottom of the Helmholtz resonant cavity. After amplification of the sound wave pressure by the HR, vibrations are generated on the PVDF film, resulting in a potential difference between the two metal electrodes. Fig. 4 shows the PVDF film and its installation.

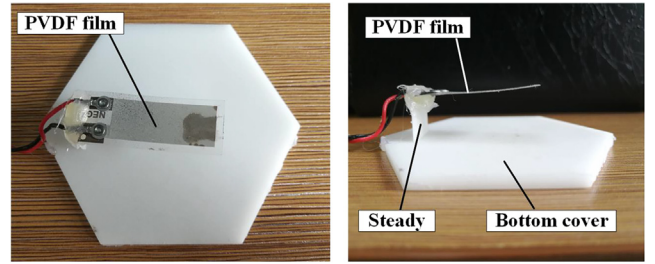


Fig. 4. The PVDF film's installation.

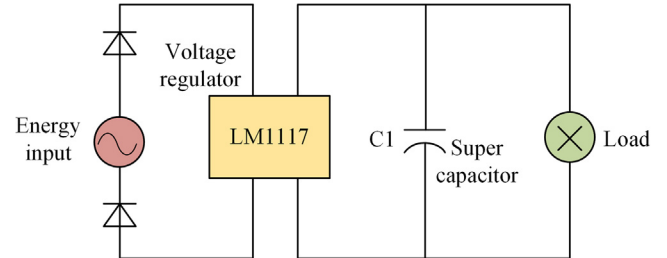


Fig. 5. Rectifying circuit for the AEHNB.

### 2.3. Power storage module

For getting a continuous output of a stable current, a power storage module was built into the proposed system, and a rectifying circuit was designed, as shown as Fig. 5. Supercapacitors were selected to store the electric energy due to its high-power density, short charge and discharge times, long cycle life and wide range of operating temperature. The sound vibrations generate an alternating current, and the electricity is stored in the super capacitor as a DC through a circuit with a rectifier. The stored energy can be applied to multiple uses, such as monitoring, emergency lights, and sensors. Fig. 6 shows the electric circuit for the AEHNB.

According to the analysis above, a prototype of the AEHNB was physically produced as shown as Fig. 7(a). And Fig. 7(b) shows the installation of the AEHNB where the vicinity is residential area. Compared with the conventional sound barrier, the AEHNB can collect the sound energy from the running high-speed trains while reducing the noise to the neighbourhood.

In the literature [36], at a distance of 25.0 m from the high-speed rail centre line, the noise level can reach more than 90 dB in many countries. TGV Reseau in France has a noise level of 97 dB at a speed of 350 km/h [37]. CRH in China has a noise level of 92 dB at a speed of 347 km/h. Considered the closer installation position along HSR, the noise barrier will receive a higher noise level. Accordingly, in this paper, the sound at 100 dB SPL is used as input condition for analysis and experiment.

## 3. Modelling and analysis of the system

### 3.1. Helmholtz resonator

The air in the neck part can be regarded as a mass vibrating with the incident sound waves, while the air in the container is expanded and

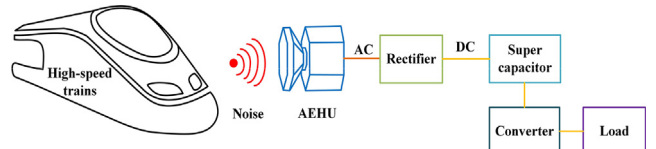
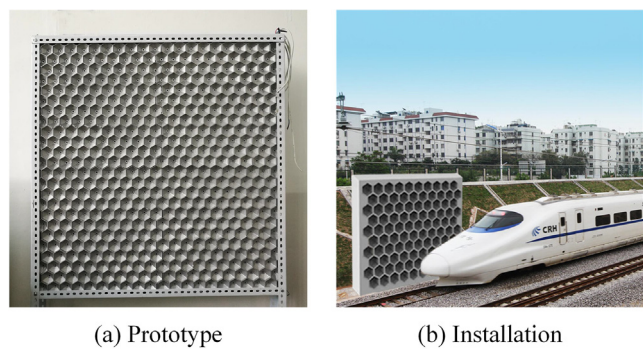


Fig. 6. Electric circuit for the AEHNB.



**Fig. 7.** Prototype and installation of the noise barrier.

$$A = \frac{P_{cavity}}{P_{incident}} = 2\pi \sqrt{\frac{(L_n V)^3}{S_n^3}} \quad (4)$$

When the HR is excited by an incident sound wave at the basic resonance frequency, the acoustic energy is harvested in the form of a resonant standing wave inside the HR. The acoustic pressure  $p(z)$  and longitudinal particle velocity  $v(z)$  are expressed as

$$p(z) = p_0 \sin \frac{\pi}{2(l_n + h)} z \quad (5)$$

$$v(z) = v_0 \cos \frac{\pi}{2(l_n + h)} z \quad (6)$$

where  $z$  is the distance from the HR open inlet.  $v_0$  is the maximum value of particle velocity at the HR open inlet.  $p_0$  is the maximum sound pressure at the bottom of the HR.

### 3.2. Acoustic energy conversion by PVDF film

When the direction of the polarization and the direction of the external force are the same or different, the PVDF film generates electricity in different ways, the 31-piezoelectric mode or 33-piezoelectric mode. When a PVDF film is installed at the bottom of the HR, the sound pressure at the two sides of the film is as shown in Fig. 9. The vibrations of the PVDF film is caused by the difference of the sound pressure  $\Delta p = p_1 - p_2$ , at the basic resonance frequency. And PVDF film generates electricity in the 31-piezoelectric mode.

$$\sigma_{in} = \sigma_i + \sigma_d + \sigma_s + \sigma_p \quad (7)$$

where  $\sigma_{in}$  is the input stress,  $\sigma_i$  is the inertance stress,  $\sigma_d$  is the damping stress,  $\sigma_s$  is the stiffness stress and  $\sigma_p$  is the equivalent stresses of the PVDF film piezoelectric element. The input stress  $\sigma_{in}$  can be regarded as the average normal stress, which is given as

$$\sigma_{in} = \frac{1}{a} \int_0^a \frac{Mp(x)d_m}{I} dx \quad (8)$$

where  $I$  is the moment of inertia of the PVDF film,  $I = 2(bd^3/12 + bdd_m^3)$ ,  $b$  is the width of the PVDF film,  $d$  is the thickness of the PVDF layer,  $d_m$  is the distance from the neutral axis to the centre of the PVDF layer, and  $a$  is the total length of the PVDF film. The equivalent bending moment  $M_p(x)$  is caused by the sound pressure difference  $\Delta p$ .

**Fig. 10** shows, at a uniform acoustic pressure, the PVDF film with distributed mass can be regarded as a plate with an equivalent point

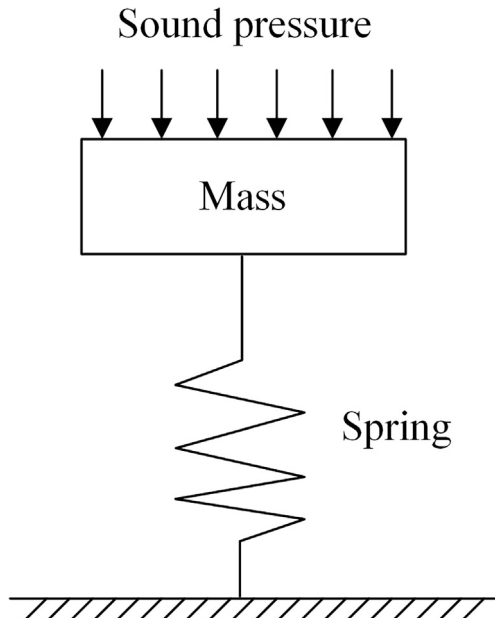


**Fig. 8.** The mass-spring model.

shrunk due to the vibrations of the air through the neck. Then, it can be seen as a spring, and the HR is the same as a mass spring system, as shown as Fig. 8.

The basic resonance frequency of the HR in response to the incident sound pressure crossing the neck is given in [38].

$$f = \frac{c}{2\pi} \sqrt{\frac{S_n}{VL_n}} \quad (1)$$

$$S_n = \pi R_n^2 \quad (2)$$

$$V = \left( \frac{3\sqrt{3}}{2} \right) l^2 h \quad (3)$$

where  $f$  is the basic resonance frequency of the HR,  $c$  is the speed of sound in the air,  $S_n$  is the cross-section area of the neck,  $V$  is the volume of cavity,  $L_n$  is the effective length of neck,  $R_n$  is the radius of the neck,  $h$  is the height of the hexagonal prisms cavity and  $l$  is the side length value of the regular hexagon.

The HR in the system is utilized to amplify the sound pressure with the proximity of noise at the resonance frequency. When the HR is excited at the resonance frequency, the incident sound pressure is amplified resonantly to obtain the peak value of the sound pressure output in the cavity. The pressure amplification factor  $A$  stands for the ratio of the sound pressure in the cavity to the incident sound pressure, which is represented as in [38].

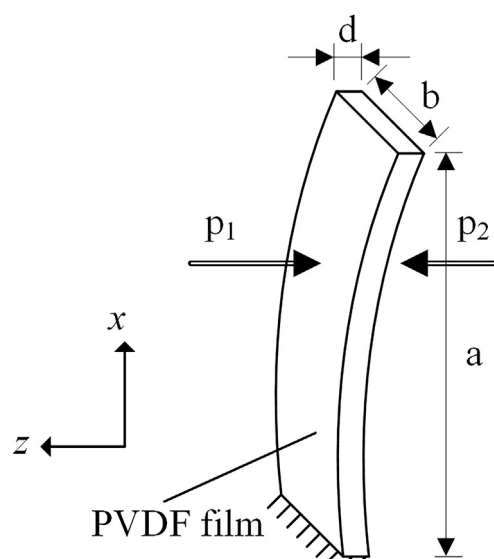


**Fig. 9.** The PVDF film vibrated by the sound pressure difference.

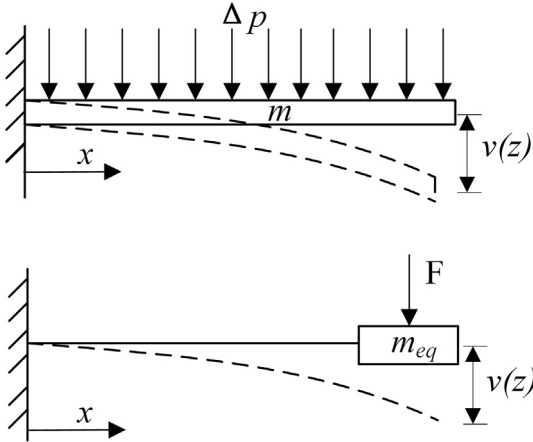


**Fig. 10.** Sketch of the PVDF film cantilever plate equivalent conversion.

mass  $m_{eq}$  under the action of force  $F$ .

The PVDF film displacement  $S(x)$  caused by the sound pressure difference  $\Delta p$  is given as

$$S(x) = \frac{bx^2(6a^2 + 4ax + x^2)}{24YI} \Delta p \quad (9)$$

where  $Y$  is the Young's modulus of the PVDF film.

$$\Delta p = p_0 [\sin(\pi(z_p + d/2)/(2(l_n + h))) - \sin(\pi(z_p - d/2)/(2(l_n + h)))] \quad (10)$$

where  $z_p$  is the distance from the HR open inlet to the PVDF film.

The kinetic energy  $G_k$  can be obtained as

$$G_k = \int_0^a dG_k = \int_0^a \frac{\dot{S}(x)^2}{2} \frac{mdx}{a} = \frac{\dot{S}(a)^2}{2} 0.257m \quad (11)$$

where  $m$  is the total mass of the PVDF film. Due to  $G_k$  can be expressed as  $\frac{\dot{S}(a)^2}{2} m_{eq}$ ,  $m_{eq}$  is equal to 0.257 m.

The induced stresses of the PVDF film piezoelectric element are expressed as

$$\sigma_i = \frac{m_{eq}}{c_1} \ddot{\delta}, \quad (12)$$

$$\sigma_d = \frac{\beta}{c_2} \dot{\delta}, \quad (13)$$

$$\sigma_s = Y\delta, \quad (14)$$

$$\sigma_p = \frac{-d_{31}Y}{d} V, \quad (15)$$

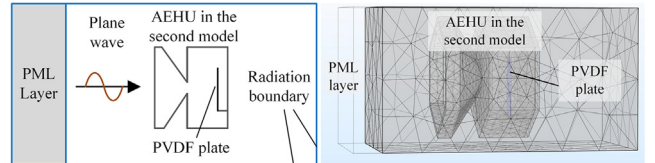
where  $\delta$  is the strain,  $d_{31}$  is the piezoelectric constant, the damping coefficient is  $\beta = 2\zeta\omega_n m_{eq} c_2 / c_1$ ,  $\zeta$  is the damping ratio, the geometric constant is  $c_1 = 3I/a^3$ ,  $c_2 = 3d/(2a^2)$  and  $\omega_n$  is undamped natural frequency. Substituting Eqs. (8) and (12)–(15) into Eq. (7), the output voltage  $V_{out}$  of the PVDF film is given as

$$V_{out} = \frac{\omega_n R C_p d_{31} d / \varepsilon}{\sqrt{R^2 C_p^2 \omega_n^2 (4\zeta^2 + k^2) + 4\zeta^2 + 4\zeta^2 \omega_n R C_p}} * \left( \frac{da^2 b}{6I} \right) \Delta p \quad (16)$$

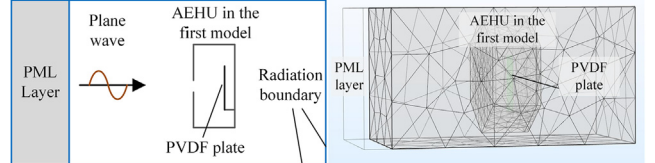
where  $k$  is the piezoelectric coupling coefficient,  $C_p$  is the piezoelectric capacitance,  $R$  is the loading resistance and  $\varepsilon$  is the permittivity. The output electric power  $P$  of the PVDF film is expressed as

$$P = \frac{V_{out}^2}{R} = \frac{(\omega_n d^2 / \varepsilon)^2 R C_p^2}{\omega_n^2 R^2 C_p^2 (4\zeta^2 + k^2) + 4\zeta^2 + 4k^2 \zeta \omega_n R C_p} * \left( \frac{da^2 b}{6I} \right) \Delta p \quad (17)$$

An optimal resistance is existed when  $\partial P / \partial R = 0$  to get the maximum power,  $R_{lop}$  is calculated as



(a) Schematic of the simulation conditions and the finite element mesh for the AEHU in the first model



(b) Schematic of the simulation conditions and the finite element mesh for the AEHU in the second model.

**Fig. 11.** System simulation of the AEHU.

$$R_{lop} = \frac{1}{\omega_n C_p} \frac{2\zeta}{\sqrt{4\zeta^2 + k^2}} \quad (18)$$

### 3.3. System simulation

The system simulation was executed using **COMSOL Multiphysics 5.3** to perform a finite element analysis. With the purpose of simulating the acoustic energy harvesting from travelling sound waves, the AEHU was in a cuboid domain, which is set as the sound field. And the sound waves can travel and leave in the sound field. The outer boundary of the cuboid domain acts as a radiation boundary that can minimize the sound wave reflection. Additionally, another cuboid domain is added to the surface of the cuboid domain where a plane wave generates, and it is set as a perfect matched layer (PML) to absorb the sound radiation generated by the air motion near the AEHU inlet. The PVDF film cantilever plate is installed at the tube bottom of the AEHU. For the AEHUs with or without the noise collection input module, two models with different resonators were compared in this paper. The simulations of the AEHU in the first model, which means without the noise collection input module, is shown in Fig. 11(a). Additionally, in order to show the effect of the noise collection input module, simulations of the AEHU in the second model, which means with the noise collection input module, was performed as shown in Fig. 11(b).

### 4. Experimental details

A prototype of the acoustic energy harvesting noise barrier was built. The overall experimental setup is shown in Fig. 12, and the experimental schematic model and details are shown in Fig. 12(a) and (b) respectively. As shown in Fig. 12, we used the speakers to simulate a certain frequency of noise to verify our proposed methods. The tests were conducted in the laboratory of thermal power and automotive engineering at Southwest Jiaotong University, and the overview of the experimental framework is shown in Fig. 13(a). Due to the limited experimental conditions, a unit of the noise barrier was used to approximately illustrate the effect of an integrated unit noise barrier. The prototype that was manufactured for the test is shown in Fig. 13(b) and (c). The PVDF film was installed on the bottom of the prototype with its plane approximately perpendicular to the direction of the incoming sound waves. The bottom cover is fixed on the bottom of the body, which forms a Helmholtz resonance cavity inside of the prototype. A DS1102E digital oscilloscope from RIGOL was used to record the voltage signal from the generator, as shown as Fig. 13(e). Two microphones (MPA201 S/N: 550507 SENS: 49.0 mV/Pa), as shown as Fig. 13(f), were settled at the entrance to the unit, in the HR, and behind the unit. The microphones were connected to a data acquisition

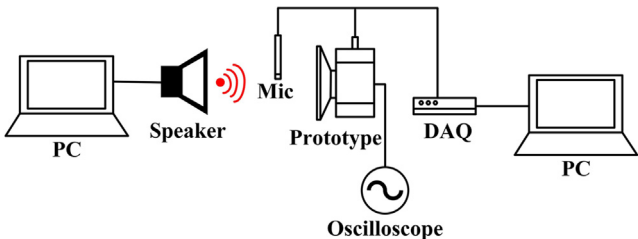


Fig. 12. Experimental setup.

device (DAQ, LMS SCADAS Mobile from SIEMENS, Fig. 13(d)) to record the sound pressure data before, during and after the system test, respectively. The output data of the sound pressure was recorded using a DAQ card and LMS Test.Lab software, shown in Fig. 13(g), and the electrical voltage was shown by a display on the screen of the oscilloscope. The data analysis process is shown in Fig. 13(h).

## 5. Results and discussion

### 5.1. Acoustic resonance in the AEHU

The characteristics of HR have been described. The HR is designed with the basic acoustic resonance frequency of 550 Hz.

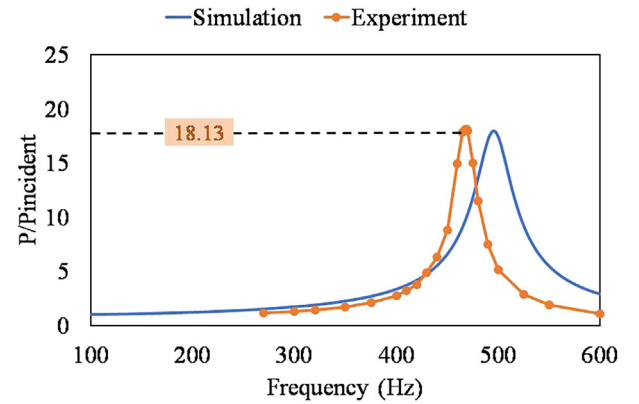


Fig. 14. The frequency response for the AEHU at first model.

In both the simulations and experiments, the incident sound is set as 100 dB SPL. To ensure that the resonators were excited resonantly, the incident sound frequency ranged widely from 100 Hz to 600 Hz in the simulations and 270 Hz to 600 Hz in the experiments. And both of the frequency ranges contain the resonance frequencies.

For the AEHU in the first model, without the noise collection input module, the result of the simulation shows an amplification ratio of 17.91 in the resonator at the frequency of 496 Hz, while the experiments show an amplification ratio of 18.13 in the resonator at the frequency of 468 Hz, as shown in Fig. 14.

For the AEHU in the second model, with the noise collection input module, the results of the simulations show an amplification ratio of 18.62 in the AEHU at the frequency of 464 Hz, while the experiment shows an amplification ratio is 20.86 at 447 Hz, as shown in Fig. 15.

From the two figures, the scatters of the experimental data approximately agree with the simulation curve, and the highest sound pressure magnification occurs near the resonance frequency. For the similar trends of the simulation and experiment, the influence of the lack of frequencies less than 270 Hz can be ignored. The differences of the resonance frequency among the calculation, simulation and experiment are 64 Hz and 28 Hz for the AEHU in the first model, while the difference between the simulations and experiments is 19 Hz for the

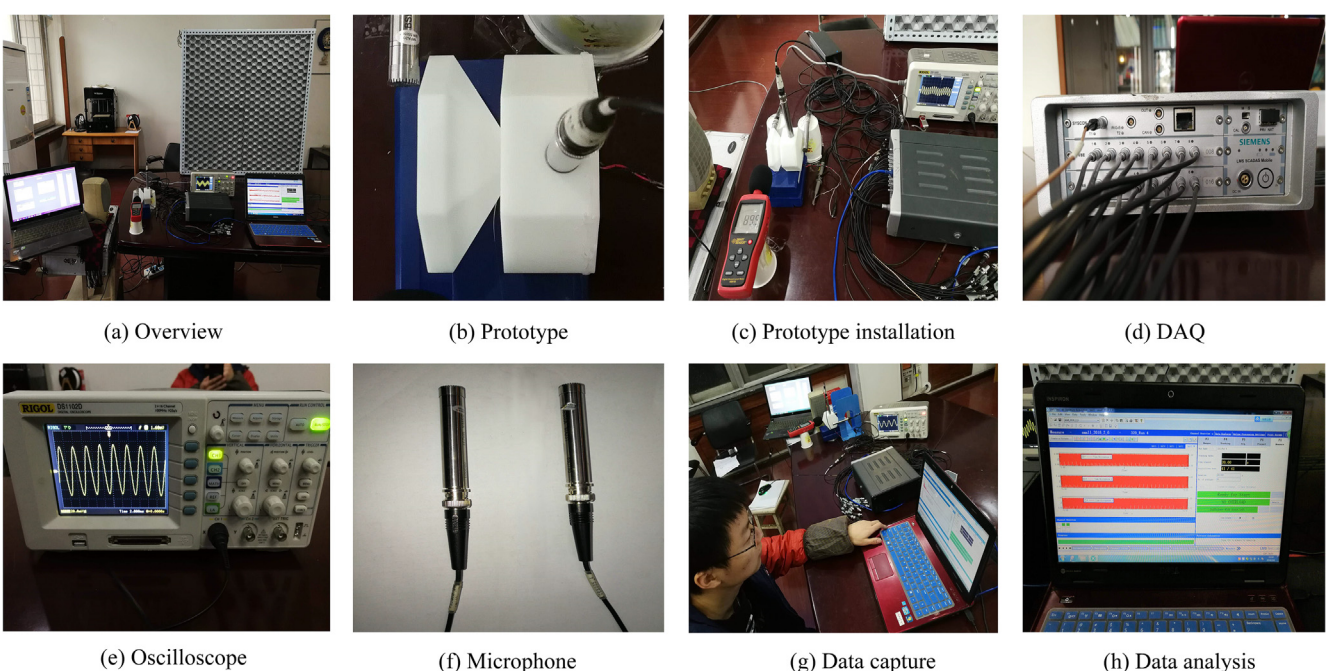


Fig. 13. Bench tests of the proposed acoustic energy harvesting noise barrier.

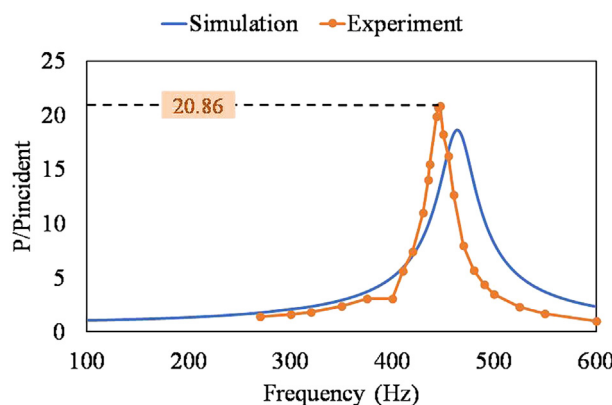


Fig. 15. The frequency response for the AEHU in the second model.

AEHU in the second model. Analysis mainly suggest that the experiment deviation was the result of the generation of environmental noise, the influence of temperature and the installation positions of the microphones, which effected the air flow rate. According to the comparison of the frequency response between the two models of the AEHU. The results show that the AEHU in the second model can achieve a higher sound pressure magnification, which means that more acoustic energy is gathered in the resonator.

## 5.2. The electricity generated by a PVDF film

The PVDF film was fixed at the bottom of the AEHU to receive the resonant sound wave in the resonator. The deformation of the PVDF film caused by the sound pressure generates electricity. From the measured voltage, the output power was obtained using  $V^2/R_{Lop}$  with an optimized resistance of  $R_{Lop} = 4$  (6 kΩ). Fig. 16 shows an example of the simulated displacement and output voltage of the AEHU in the first model, without the noise collection input module. The comparison between the experimental data and the simulated results is shown in Fig. 17. For the AEHU in the first model, when the PVDF film is vibrated by the resonant sound pressure, the simulated voltage and power are 47.26 mV and 0.48 μW at an incident frequency of 496 Hz, while 42.10 mV and 0.38 μW are measured at 468 Hz in the experiments.

Fig. 18 shows an example of the simulated displacement and output voltages of the AEHU in the second model. The comparison between the experimental data and the calculated results is shown in Fig. 19. The results show that the simulated voltage and power are 49.13 mV and 0.52 μW at an incident frequency of 464 Hz, while 52.20 mV and 0.59 μW are measured at 445 Hz. in the experiments.

The comparison shows the effect of the noise collection input module, which can collect more of the energy of the noise. This fact means that the AEHU in second model can harvest more acoustic

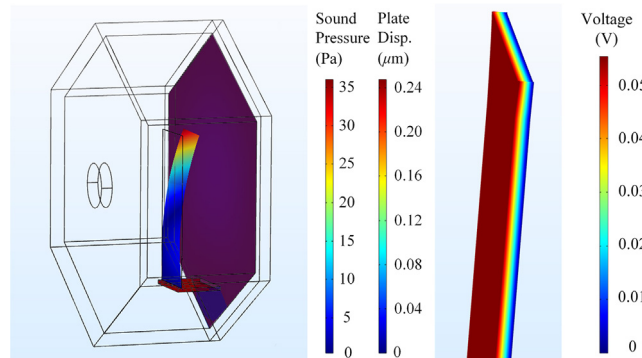


Fig. 16. An example of the simulated displacement and output voltage of the AEHU in the first model.

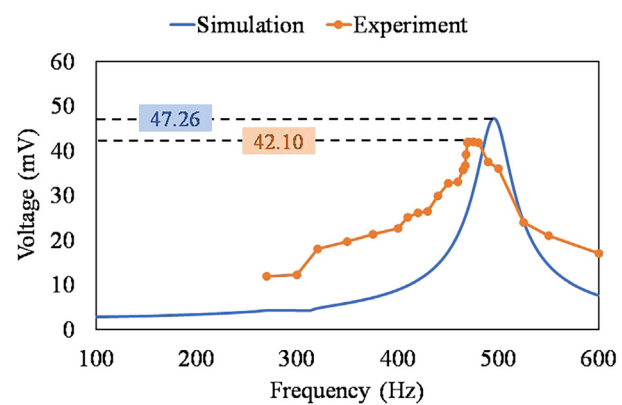


Fig. 17. Comparison between the experimental and simulated voltages of the AEHU at different frequencies in the first model.

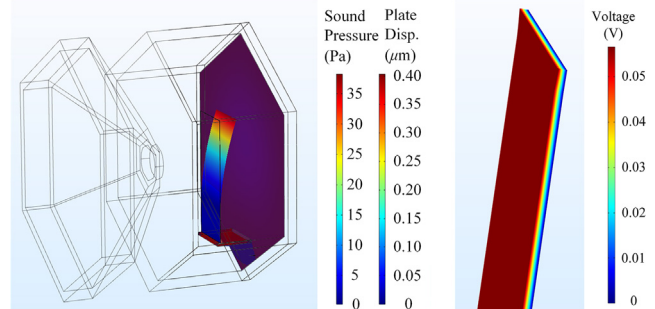


Fig. 18. An example of the simulated displacement and output voltages of the AEHU in the second model.

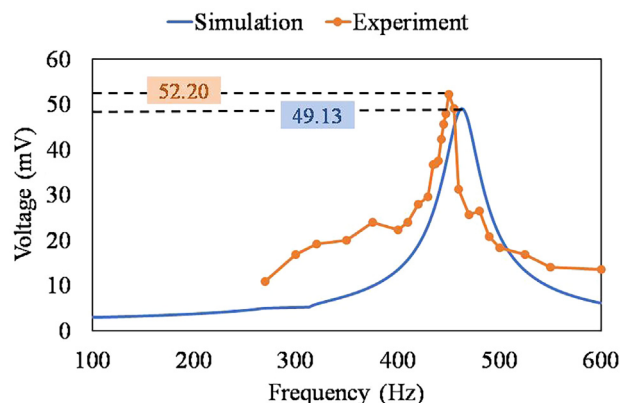


Fig. 19. The comparison between the experimental and simulated voltages of the AEHU at different frequencies in the second model.

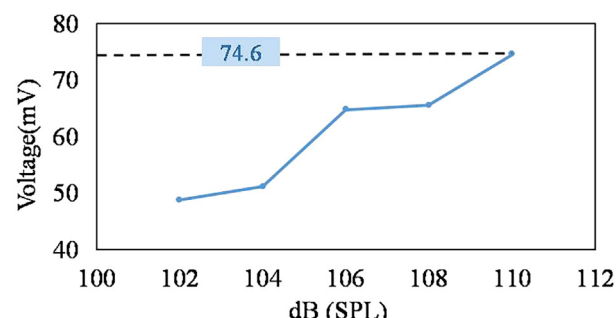


Fig. 20. Experimental voltage of the AEHU in the second model at 447 Hz in different SPL.

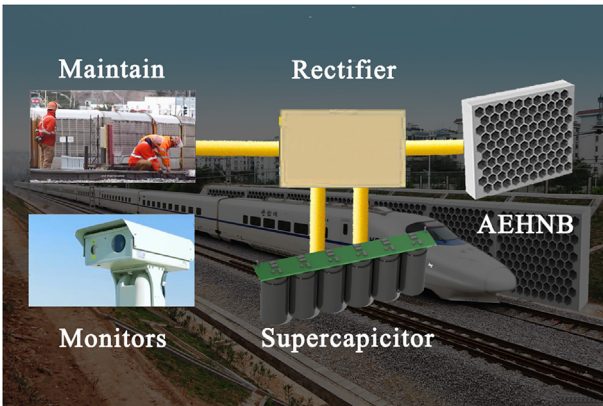


Fig. 21. Application of the AEHNBs in high-speed railways.

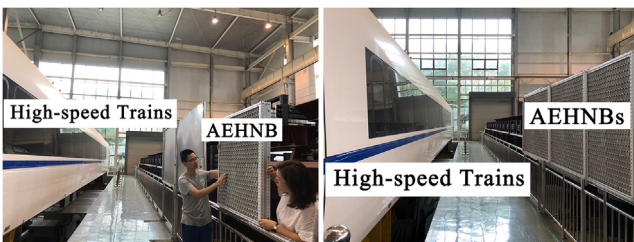


Fig. 22. Experimental environment of the AEHNBs.

energy. Fig. 20 shows the experimental voltage of the AEHU in the second model at 447 Hz from 100 dB SPL to 110 dB SPL, and a voltage of 74.6 mV and 1.24  $\mu$ W can be measured at 110 dB SPL.

### 5.3. The electricity generation of an AEHNB

A prototype of the AEHNB was manufactured, it was 1.5 m long and 1.3 m wide, which combines 24 × 20 AEHUs in the second model together as shown in Fig. 14(a). The expected instantaneous output voltage peak of the AEHNB can reach 25.1 V at the incident sound at 100 dB SPL, and 35.8 V at 110 dB SPL. Compared to existing noise barrier, the AEHNB can achieve noise reduction and electricity generation synchronously.

As shown in Fig. 20, the AEHNBs are installed along high-speed railways where the vicinity is residential area. The noise of passing-by high-speed trains actuates the AEHNBs, which collect the acoustic energy of noise and store the energy in the supercapacitor, while reducing the noise. As the development of railway systems, the proposed AEHNBs could be a reliable solution for powering some small electronic devices and for standby power supplies, such as railway monitors and maintenance.

Furthermore, Fig. 21 shows the Experimental environment of the AEHNBs in State-Key Laboratory of Traction Power, Southwest Jiaotong University, which provides feasibility for subsequent optimization and evaluation of system performance (see Fig. 22).

## 6. Conclusion

In this paper, a renewable low frequency acoustic energy harvesting noise barrier is reasonably, systematically and successfully developed for high-speed rails. The proposed system provides a practical method of energy supply for low power electronic devices along a high-speed rail. For the purposes of noise reduction and electricity generation, the proposed system converts sound energy to electricity using a Helmholtz resonator and a PVDF (Polyvinylidene Fluoride) film. The renewable energy application scheme consists of four main components: the noise collection input module, the sound pressure amplification module, the

electricity generator module and the power storage module.

The resonant frequency and amplification ratio of the acoustic energy harvesting unit in the first model are measured as 468 Hz and 18.13, while the resonant frequency and amplification ratio of the acoustic energy harvesting unit in the second model are measured as 447 Hz and 20.86. To convert the incident acoustic energy, the PVDF film has been placed at the bottom of the acoustic energy harvesting unit. With the amplification of sound pressure, the voltage and power can be obtained at a certain resonance frequency. Through the experiments, the acoustic energy harvesting unit in the second model which includes the noise collection input module has a better performance, and the maximum voltage and power are 52.20 mV and 0.59  $\mu$ W with an incident SPL of 100 dB. The output voltage increases with the increase of the incident sound pressure. At an incident SPL of 110 dB, a voltage of 74.6 mV has been measured which corresponds to a power of 1.24  $\mu$ W. As the prototype of the acoustic energy harvesting noise barrier manufactured by this paper integrates multiple acoustic energy harvesting unit arrays, the total voltage can reach 35.8 V at 110 dB SPL. Therefore, the acoustic energy harvesting noise barrier can be applied to HSR to replace the conventional noise barrier, especially near residential areas in the future.

## Acknowledgments

This work was supported by the National Natural Science Foundation of China under Grant No. 51675451, by the Science and Technology Projects of Sichuan and Chengdu under Grant Nos. 2016GZ0026, 2016CC0027, 2017RZ0056 and 18MZGC0272. The first three authors contributed equally to this work. The asterisk indicates the author to whom all correspondence should be directed.

## Appendix A. Supplementary material

Supplementary data associated with this article can be found, in the online version, at <https://doi.org/10.1016/j.apenergy.2018.08.080>.

## References

- [1] Campos J, Rus GD. Some stylized facts about high-speed rail: a review of HSR experiences around the world. *Trans Policy* 2009;16(1):19–28.
- [2] Zhang XT, Pan HY, Qi LF, Zhang ZT, Yuan YP, Liu YJ. A renewable energy harvesting system using a mechanical vibration rectifier (MVR) for railroads. *Appl Energy* 2017;204:1535–43.
- [3] Vickerman R. High-speed rail in Europe: experience and issues for future development. *Ann Region Sci* 1997;31(1):21–38.
- [4] Mallet C, Létourneau F, Poisson F, Talotteb C. High speed train noise emission: Latest investigation of the aerodynamic/rolling noise contribution. *J Sound Vib* 2006;293(3):535–46.
- [5] Liu MY, Lin R, Zhou SX, Yu YL, Ishida A, McGrath M, et al. Design, simulation and experiment of a novel high efficiency energy harvesting paver. *Appl Energy* 2018;212:966–75.
- [6] Reiter P, Wehr R, Ziegelwanger H. Simulation and measurement of noise barrier sound-reflection properties. *Appl Acoust* 2017;123:133–42.
- [7] Arenas JP. Potential problems with environmental sound barriers when used in mitigating surface transportation noise. *Sci Total Environ* 2008;405(1–3):173–9.
- [8] Dincer I, Acar C. Smart energy systems for a sustainable future. *Appl Energy* 2017;194:225–35.
- [9] Ju X, Xu C, Han X, Du XZ, Wei GS, Yang YP. A review of the concentrated photovoltaic/thermal (CPVT) hybrid solar systems based on the spectral beam splitting technology. *Appl Energy* 2017;187:534–63.
- [10] Zhang P, Li WY, Li S, Wang Y, Xiao WD. Reliability assessment of photovoltaic power systems: review of current status and future perspectives. *Appl Energy* 2013;104:822–33.
- [11] Nordmann T, Clavadetscher L. PV on noise barriers. *Prog Photovolt Res Appl* 2004;12(6):485–95.
- [12] Schepper ED, Passel SV, Manca J, Thewys T. Combining photovoltaics and sound barriers – a feasibility study. *Renew Energy* 2012;46:297–303.
- [13] Faturochman GJ, Jong MMD, Santbergen R, Folkerts W, Zemana M, Smets AHM. Maximizing annual yield of bifacial photovoltaic noise barriers. *Sol Energy* 2018;162:300–5.
- [14] Gu MA, Liu YS, Yang JJ, Peng L, Zhao CL, Yang ZL, et al. Estimation of environmental effect of PVNB installed along a metro line in China. *Renew Energy* 2012;45:237–44.
- [15] Zhang ZT, Zhang XT, Rasim YB, Wang CB, Du B, Yuan YP. Design, modelling and

- practical tests on a high-voltage kinetic energy harvesting (EH) system for a renewable road tunnel based on linear alternators. *Appl Energy* 2016;164:152–61.
- [16] Zhang ZT, Zhang XT, Chen WW, Rasim Y, Salman W, Pan HY, et al. A high-efficiency energy regenerative shock absorber using supercapacitors for renewable energy applications in range extended electric vehicle. *Appl Energy* 2016;178:177–88.
- [17] Wang H, Jasim A, Chen XD. Energy harvesting technologies in roadway and bridge for different applications – a comprehensive review. *Appl Energy* 2018;212:1083–94.
- [18] Orrego S, Shoele K, Ruas A, Doran K, Caggiano B, Mittal R, et al. Harvesting ambient wind energy with an inverted piezoelectric flag. *Appl Energy* 2017;194:212–22.
- [19] Voccia H, Neri I, Travasso F, Gammaitoni L. Kinetic energy harvesting with bistable oscillators. *Appl Energy* 2012;97:771–6.
- [20] Zhang XT, Zhang ZT, Pan HY, Salman W, Yuan YP, Liu YJ. A portable high-efficiency electromagnetic energy harvesting system using supercapacitors for renewable energy applications in railroads. *Energy Convers Manage* 2016;118:287–94.
- [21] Guo LK, Lu Q. Modeling a new energy harvesting pavement system with experimental verification. *Appl Energy* 2017;208:1071–82.
- [22] Roshani H, Dessouky S, Montoya A, Papagiannakis AT. Energy harvesting from asphalt pavement roadways vehicle-induced stresses: a feasibility study. *Appl Energy* 2016;182:210–8.
- [23] Guan MJ, Liao WH. Design and analysis of a piezoelectric energy harvester for rotational motion system. *Energy Convers Manage* 2016;111:239–44.
- [24] Abdelmoula H, Sharpe N, Abdelkefi A, Lee H, Priya S. Low-frequency Zigzag energy harvesters operating in torsion-dominant mode. *Appl Energy* 2017;204:413–9.
- [25] Li B, Laviage AJ, You JH, Kim YJ. Harvesting low-frequency acoustic energy using multiple PVDF beam arrays in quarter-wavelength acoustic resonator. *Appl Acoust* 2013;74(11):1271–8.
- [26] Pillai MA, Deenadayalan E. A review of acoustic energy harvesting. *Int J Precis Eng Man* 2014;15(5):949–65.
- [27] Zhou ZY, Qin WY, Zhu P. Harvesting acoustic energy by coherence resonance of a bi-stable piezoelectric harvester. *Energy* 2017;126:527–34.
- [28] Hu ZH, Yang C, Cheng L. Acoustic resonator tuning strategies for the narrowband noise control in an enclosure. *Appl Acoust* 2018;134:88–96.
- [29] Liu F, Phipps A, Horowitz S, Ngo K, Cattafesta L, Nishida T, et al. Acoustic energy harvesting using an electromechanical Helmholtz resonator. *J Acoust Soc Am* 2008;123(4):1983–90.
- [30] Yuan M, Cao ZP, Luo J, Zhang JY, Chang C. An efficient low-frequency acoustic energy harvester. *Sensor Actuat A-Phys* 2017;264:84–9.
- [31] Kim SH, Ji CH, Galle P, Herrault F, Wu XS, Lee JH, et al. An electromagnetic energy scavenger from direct airflow. *J Micromech Microeng* 2009;19(9):094010. [8 pages].
- [32] Noh S, Lee H, Choi B. A study on the acoustic energy harvesting with Helmholtz resonator and piezoelectric cantilevers. *Int J Precis Eng Man* 2013;14(9):1629–35.
- [33] Chanaud RC. Effects of geometry on the resonance frequency of Helmholtz resonators. *J Sound Vib* 1994;178(3):337–48.
- [34] Liu ZQ, Zhan JX, Fard M, Davy JL. Acoustic properties of a porous polycarbonate material produced by additive manufacturing. *Mater Lett* 2016;181:296–9.
- [35] Cahill P, Nuallain NAN, Jackson N, Mathewson A, Karoumi R, Pakrashi V. Energy harvesting from train-induced response in bridges. *J Bridge Eng* 2014;19(9):04014034. [10 pages].
- [36] Wakabayashi Y, Kurita T, Yamada H, Horiuchi M. Noise measurement results of Shinkansen high-speed test train (FASTECH360S,Z). In: Proceedings of the 9th International Workshop on Railway Noise, Munich, Germany, September 4–8; 2007.
- [37] Poisson F, Gautier PE, Letourneau F. Noise sources for high speed trains: a review of results in the TGV Case. In: Proceedings of the 9th International Workshop on Railway Noise, Munich, Germany, September 4–8; 2007.
- [38] Blackstock DT, Atchley AA. Fundamentals of physical acoustics. *J Acoust Soc Am* 2001;109(4):1274–6.